Journal of Process Control 76 (2019) 74–86

Contents lists available at ScienceDirect

Journal of Process Control

journal homepage: www.elsevier.com/locate/jprocont

Modelling and predictive control of a solar cooling plant with flexible configuration

Niraj Rathod [a], Alessio La Bella [a,*], Gianluca Puleo [a], Riccardo Scattolini [a], Andrea Rossetti [b], Carlo Sandroni [b]

[a] Dipartimento di Elettronica, Informazione e Bioingegneria, Politecnico di Milano, via Ponzio 34/5, 20133 Milano, Italy
[b] Power Generation Technologies and Materials Department, Ricerca Sistema Energetico, Via R. Rubattino 54, 20134 Milano, Italy

ARTICLE INFO

Article history:
Received 5 February 2018
Received in revised form 9 January 2019
Accepted 20 January 2019
Available online 26 February 2019

Keywords:
Solar cooling plant
Modelling
Model identification
Model Predictive Control (MPC)
Hybrid systems

ABSTRACT

This paper focuses on the modelling and predictive control of a real medium temperature solar cooling system made up of a solar collector, an absorption chiller, a gas heater, hot and cold water storage tanks, connecting pipes, pumps, and a number of valves, allowing to modify the plant configuration in order to optimize its performance in terms of electric power and gas consumption. A detailed model of the plant is first obtained as a mix of first principle equations, validated with data collected on the plant, and identification techniques. Then, the model is simplified and used to formulate a hybrid Model Predictive Control (MPC) problem computing the optimal plant configuration over a prediction horizon of six hours, or more, and based on the available forecast of the solar radiation and user demand. The developed MPC algorithm has been used to control the plant; some of the collected results are reported here to witness the potentialities of the proposed approach.

1. Introduction

The ongoing climate changes and their global warming effects push towards an increasing use of cooling and air conditioning systems, with consequent huge energy consumption. For the most part, this energy comes from the burning of fossil fuels with production of carbon dioxide and other gases with harmful environmental impact, see e.g. [1]. The effects of this positive feedback can be reduced by increasing the efficiency of the refrigeration units and, mainly, with a wider use of renewable energy sources. In this context, and with reference to air conditioning systems, solar cooling seems to be a promising solution, since the solar radiation is higher during the hours of the day when the demand of cooling is maximum. For these reasons, the solar cooling technology is rapidly developing, see [2–4] and [5] for the related control problems.Advanced solar cooling systems are characterized by a flexible configuration allowing to operate them at different operating modes and to guarantee a higher primary energy saving. This flexibility is typically achieved with hot and cold storages, an additional gas heater, and a number of pumps and on/off valves which allow to modify the path followed by the fluids. The management of these systems is quite challenging since many configurations can be chosen and the optimal setting depends on the weather conditions and on the user demand which are not always predictable with sufficient accuracy [6]. This task can be suitably tackled in the framework of hybrid control, where continuous variables, typically flow rates governed by pumps, must be coordinated with the proper selection of discrete (boolean) inputs, usually commands to on/off valves. The more promising tool for the solution of these control problems is Model Predictive Control (MPC), as witnessed in [7]. The MPC approach has been applied to the solar cooling plant located at the University of Seville, as reported in [8–10], whose structure and model have been extensively described in [11]. A robust supervisory control with hybrid dynamics for the same plant based on energetic aspects and several identification experiments has been reported in [12]. The hybrid modeling and control of the solar-thermal system located at the University of Almeria have been described in [13,14]. The same plant has been considered in [15,16], where a distributed MPC algorithm has been designed for the optimal management of energy distribution in buildings. The use of MPC for control of a solar cooling plant has also been considered in [17,18], where the results of a detailed simulation study are reported and discussed. An interesting solution aimed at reducing the computational burden involved by the hybrid nature of the

* Corresponding author.
E-mail addresses: niraj.rathod@mail.polimi.it (N. Rathod), alessio.labella@polimi.it (A.L. Bella), gianluca.puleo@mail.polimi.it (G. Puleo), riccardo.scattolini@polimi.it (R. Scattolini), andrea.rossetti@rse-web.it (A. Rossetti), carlo.sandroni@rse-web.it (C. Sandroni).

https://doi.org/10.1016/j.jprocont.2019.01.009
0959-1524/

Fig. 1. Experimental solar cooling plant at RSE, Milan.

problem has been proposed in [10], where a two level control structure has been proposed. At the higher layer, the analytic hierarchy process approach, see [19], is used to define the optimal plant configuration based on its internal state and weather conditions, while at the lower layer a more standard MPC problem is formulated.

This paper presents the results of a research aimed at designing a hybrid control system, based on MPC, for the solar cooling plant located at RSE (Ricerca Sistema Energetico), Milan, and shown in Fig. 1. Dynamic models of the plant devices, namely the solar collector, the storage tanks, the pipes, the chiller, and of the user are first derived. Then, a Hybrid MPC algorithm (HMPC) is designed and applied, every fifteen minutes and according to a receding horizon strategy, to compute the optimal operating mode along a future prediction horizonequal or greater than six hours. The choice of the sampling time $\tau = 15$ min is due to two considerations. First, the dynamics of the temperatures in the different sections of the plant are characterised by rise times in the range [50,90] min (see for example Figs. 12, 13 in Section 4), depending on the system configuration, so that the adopted value of τ matches the guidelines of [20]. Second, in the application here reported weather forecasts were available every fifteen minutes and for the next six hours.

The performance of the control algorithm have been tested on the real plant and compared to an already existing controller with very satisfactory results. With respect to the plants in Seville and Almeria, see [11,13], the size and the layout of the system are different, mainly due to the presence of a cold water storage tank, and to the management of the recirculating pump; moreover, in the Seville and Almeria plants the hot water loop operating temperature is much lower than the one considered here, where 200 °C can be reached. In addition, here the models of some elements, i.e. the double-effect absorption chiller and the user, have been obtained with black-box identification procedures. More in general, with respect to the previously cited literature, in the implementation here described a longer sampling time allows one to use longer prediction horizons, that, in turn, leads to look at the long term behaviour of the fluid temperatures in the storage tanks, and to reduce the frequency of switching of the system among different configurations.

The paper is organized as follows. Section 2 describes the plant, while the model of its components is derived in Section 3. The control scheme and the HMPC algorithm are described in Section 4. In Section 5 some simulation results are first discussed, then the performances of the controller applied to the real plant are described. Finally, some conclusions are drawn in Section 6.

2. Solar cooling plant

The structure of the plant is shown in Fig. 2. It consists of two main water loops: the hot water cycle is composed of the pump P001, the solar collectors and the hot storage, while the cold water cycle is composed of the pump P301, the cold tank and the air handling unit (AHU). The two water loops are connected through the absorption chiller. The solar energy received by the collectors is used to heat up the water that is either fed to the chiller or used to heat the hot storage. The chiller absorbs the energy from the hot water and it refrigerates the cold water loop in order to meet the user demand, i.e. the AHU request, or to cool down the cold storage. In case the water coming from the solar collector is not at a sufficiently high temperature, the chiller works in gas mode. The main objective of the control system is to manage the storages and the pumps to meet the user demand by minimizing the overall energy and gas consumption. The nominal operating temperature of the hot water loop varies between 150–190 °C; because of this the water is recirculated at high pressure in order to avoid evaporization. Regarding the cold water cycle, the nominal water temperature is in the range 5–17 °C so that the user demand can be properly satisfied. The sizing of the plant is done according to the design parameters reported in Table 1, see also [21].

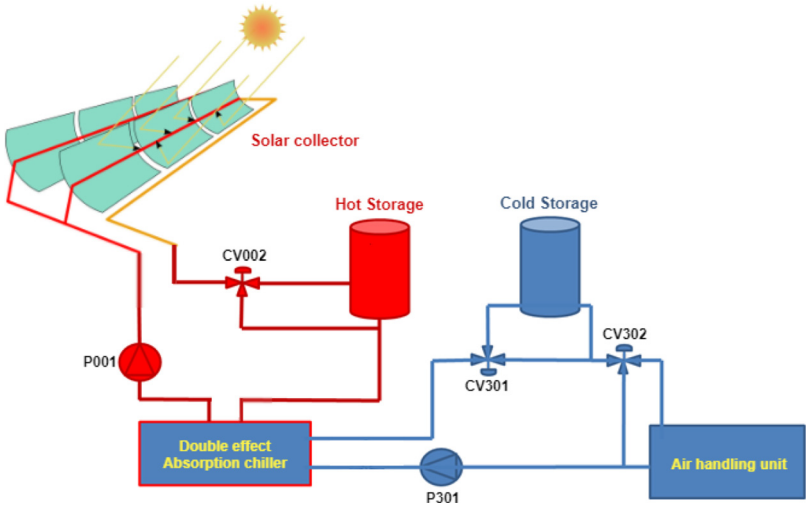

Fig. 2. Solar cooling plant. Hot water cycle (red), cold water cycle (blue). (For interpretation of the references to color in this figure legend, the reader is referred to the web version of this article).

Table 1
Solar cooling plant design parameters.

Description	Value	Unit
Water-LiBr double-effect absorption chiller power	23	kW
Maximum AHU refrigeration power	50	kW
Parabolic trough collector area	50	m^2
Heat storage volume	0.75	m^3
Cold storage volume	1.5	m^3
Hot water pipe length	69	m
Hot water pipe diameter	0.025	m
Cold water pipe length	104	m
Cold water pipe diameter	0.03	m
Volumetric Solar Pump (Gear type)	1.8	$m^3\,h^{-1}$

Table 2
Feasible plant configurations.

Mode	Description	δ_{ht}	δ_{ch}	δ_{ct}
M_1	Recirculation	0	0	0
M_2	Cooling	0	1	0
M_3	Hot tank	1	0	0
M_4	Hot tank + cooling	1	1	0
M_5	Cold tank	0	0	1
M_6	Cold tank + cooling	0	1	1
M_7	Hot tank + cold tank + cooling	1	1	1
M_8	Hot tank + cold tank	1	0	1

2.1. Operating modes

Looking again at Fig. 2, it can be noticed that acting on the on/off valves CV002 and CV301, i.e. the bypasses of the hot and cold tanks respectively, the plant can take different configurations. The positions of the valves CV002 and CV301 are indicated by the boolean variables δ_{ht} and δ_{ct}, respectively, that are set equal to 1 if the water flows through the storages, while $\delta_{ht/ct} = 0$ if the tanks are bypassed. The chiller can be switched on/off acting on the command variable δ_{ch}, which is set to 1 if the chiller is on. In summary, the feasible plant configurations are defined by the vector

$$\delta = [\delta_{ht} \quad \delta_{ch} \quad \delta_{ct}] \tag{1}$$

and are summarized in Table 2.

These operating modes are detailed below:

- M_1 –*Recirculation*: the hot water is heated by the solar collector while the chiller is switched off.
- M_2 –*Cooling*: the cold water is cooled by the chiller absorbing energy from the hot water loop or from gas combustion.
- M_3 –*Hot tank*: the hot storage is included in the loop, e.g. to accumulate hot water, while the chiller is off.
- M_4 –*Hot tank + cooling*: the hot water flows through the hot storage and then it is fed to the chiller which is cooling the cold water loop.
- M_5 –*Cold tank*: the cold storage is included in the loop, e.g. to satisfy the user demand, while the chiller is off.
- M_6 –*Cold tank + cooling*: the cold water is refrigerated by the chiller and it flows through the cold storage before being fed to the user.
- M_7 –*Hot tank + cold tank + cooling*: both storages are included and the chiller is on.
- M_8 –*Hot tank + cold tank*: both storages are included in the loop with the chiller off.

The possibility of including or excluding the storages has many benefits. For instance, it is possible to store water in the hot storage when there is high solar radiation and the user demand is low, so that it can be available for later use. In addition, it is also possible to produce cold water and store it to satisfy the demand from the user when there is no solar radiation. The flow of pump P001 can be manipulated in order to efficiently use the solar radiation; this is not the case of pump P301 whose functioning can be partially controlled. In details the pump is switched on solely in case the AHU and the chiller are operating. When the pump is switched on, it works at fixed flow $q_{cw} = 3.6\,m^3\,h^{-1}$. Finally, the valve CV302 in Fig. 2 is controlled by an (unknown) internal control based on the user demand and therefore it cannot be externally manipulated.

Table 3
Solar collector model variables and parameters.

Symbol	Description	Units
t	Time	s
x	Main space coordinate	m
ρ_m	Density of metal	$kg\,m^{-3}$
ρ_f	Density of fluid	$kg\,m^{-3}$
c_m	Specific heat capacity of metal	$J\,kg^{-1}\,°C^{-1}$
c_f	Specific heat capacity of water	$J\,kg^{-1}\,°C^{-1}$
A_m	Cross-sectional area of metal tube	m^2
A_f	Cross-sectional area of fluid	m^2
T_m	Temperature of metal	°C
T_f	Temperature of fluid	°C
q_{hw}	Volumetric flow rate of the hot water pump	$m^3\,s^{-1}$
I	Solar radiation	$W\,m^{-2}$
η_0	Mirror optical efficiency	–
η_{end}	End loss efficiency	–
G	Mirror optical aperture	m
T_a	Ambient temperature	°C
H_1	Global coefficient of thermal losses	$W\,m^{-1}\,°C^{-1}$
H_t	Coefficient of metal-fluid thermal transmission	$W\,m^{-2}\,°C^{-1}$
D_i	Inner diameter of collector tube	m

3. Plant model

In this section, the modelling and validation of the main devices of the plant is discussed in detail. All the models have been validated with data collected during the operation period of the plant.

3.1. Solar collector

The parabolic trough collector concentrates the sunlight onto a receiver pipe located along the focal line to heat the water, used as heat transfer fluid, passing through it. The dynamics of the hot water temperature flowing through the receiver pipe can be expressed by the following system of partial differential equations describing the energy balance of the metal surface and of the fluid [22]. The meaning of the model variables appearing in (2) is reported in Table 3.

$$\rho_m c_m A_m \frac{\partial T_m}{\partial t}(t,x) = \eta_0 G I(t) \eta_{end} - H_1(T_m(t,x) - T_a(t)) + - D_i \pi H_t(T_m(t,x) - T_f(t,x)) \tag{2a}$$

$$\rho_f c_f A_f \frac{\partial T_f}{\partial t}(t,x) + \rho_f c_f q_{hw}(t) \frac{\partial T_f}{\partial x}(t,x) = D_i \pi H_t(T_m(t,x) - T_f(t,x)) \tag{2b}$$

In the development of the plant simulator, these equations, and the similar ones describing the pipes introduced in the following, have been implemented by means of a finite differencing of the space variable, see [23].Specifically, the solar collector has been modeled as a series of 200 elementary volumes, each one of length $0.1025m$. In this way, the two partial differential equations (2) have been transformed into a set of ordinary differential equations with respect to time. The values of the parameters $H_1 = 7.3$ and $H_t = 600$ in (2) have been estimated from real data acquired with sampling period $12s$, while the model validation procedure has been developed considering the transients of the hot water flow rate q_{hw}, of the solar radiation I, and of the ambient temperature T_a. The input and validation data are shown in Figs. 3 and 4. The Normalized

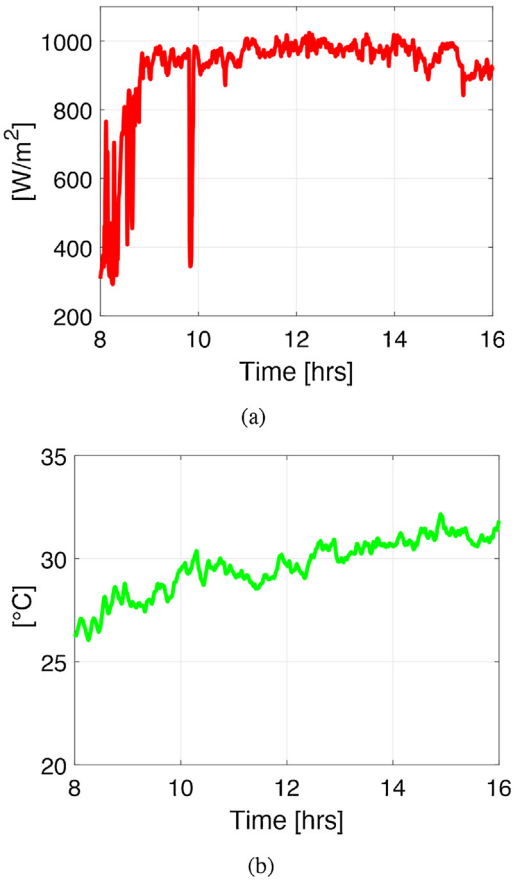

Fig. 3. Inputs to the solar collector model for validation: (a) solar radiation, (b) ambient temperature.

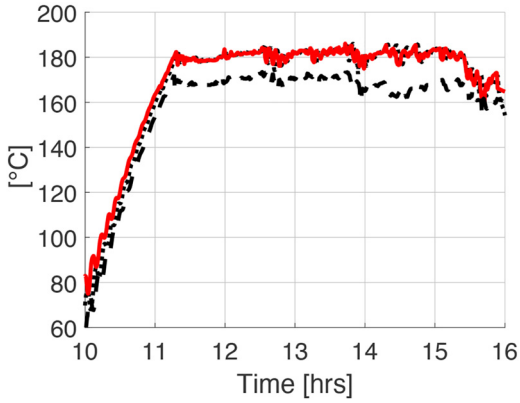

Fig. 4. Solar collector model validation: input temperature (dashed line), real output (solid line), model response (dotted line).

Mean Squared Error (NMSE) between the real and simulated temperature trends of the solar collector output is 1.23%. The model produces very good results both in transient conditions and at the steady state.

3.2. Storage tanks

For the purpose of this work, it has been sufficient to assume that inside the tanks the water volume is constant and the temperature is uniform, so that the tanks can be described by the following energy balances

Table 4
Model variables and parameters for the hot and cold storages.

Symbol	Description	Units
M_{ht}	Fluid mass of hot storage	kg
M_{ct}	Fluid mass of cold storage	kg
T_{ht}	Temperature in the hot tank	°C
T_{ct}	Temperature in the cold tank	°C
q_{cw}	Volumetric flow rate to the cold water pump	$m^3\ s^{-1}$
T_{ht}^{in}	Input temperature to the hot tank	°C
T_{ct}^{in}	Input temperature to the cold tank	°C
T_a	Environmental temperature	°C
H_{ht}	Coefficient of thermal losses of hot storage	$W\ m^{-2}\ °C^{-1}$
H_{ct}	Coefficient of thermal losses of cold storage	$W\ m^{-2}\ °C^{-1}$
A_{ht}	External surface area of the hot tank	m^2
A_{ct}	External surface area of the cold tank	m^2

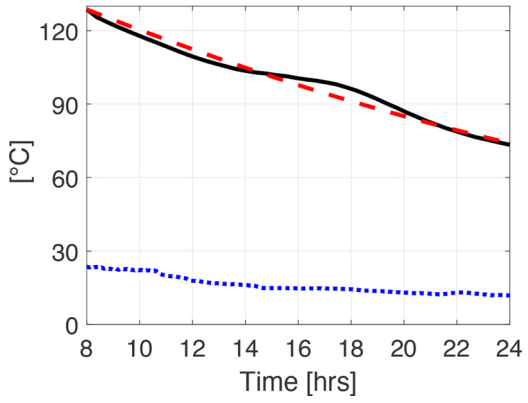

Fig. 5. Hot tank model validation: ambient temperature (dotted line), real tank temperature (solid line), model response (dashed line).

Hot tank

$$c_f M_{ht} \frac{dT_{ht}(t)}{dt} = \delta_{ht}(t)\, q_{hw}(t)\, c_f\, \rho_f (T_{ht}^{in}(t) - T_{ht}(t)) + - H_{ht} A_{ht} (T_{ht}(t) - T_a(t)) \quad (3)$$

Cold tank

$$c_f M_{ct} \frac{dT_{ct}(t)}{dt} = \delta_{ct}(t)\, q_{cw}(t)\, c_f\, \rho_f (T_{ct}^{in}(t) - T_{ct}(t)) + - H_{ct} A_{ct} (T_{ct}(t) - T_a(t)) \quad (4)$$

where the adopted symbols are described in Table 4. Note that the first terms at the right hand side of each equation are taken into account only if the storages are included in the loop, as specified by the status of the boolean variables δ_{ht} and δ_{ct}.

The models of the hot (cold) storage tanks have been validated by first heating (cooling) the stored water to some temperature value and then leaving it to cool down (heat up) for several hours. In this way it has been possible to estimate the coefficients $H_{ht} = 6 \cdot 10^{-3}$ and $H_{ct} = 2.8 \cdot 10^{-3}$ in (3), (4). The validation result concerning the hot water tank is shown in Fig. 5, it can be seen that the model temperature output fits satisfactorily the measured data (NMSE = 1.8%). This proves that the simplifying assumption of uniform temperature inside the tank is acceptable. A more detailed model could easily be obtained assuming a stratification of the temperature profile inside the tank. Similar results, not reported here for the sake of compactness, have been obtained for the cold water tank.

3.3. Pipes

The pipes have been modelled in the same way of the solar collector by means of energy balance equations, see (2), excluding the term related to solar radiation, since its effect is negligible, as well

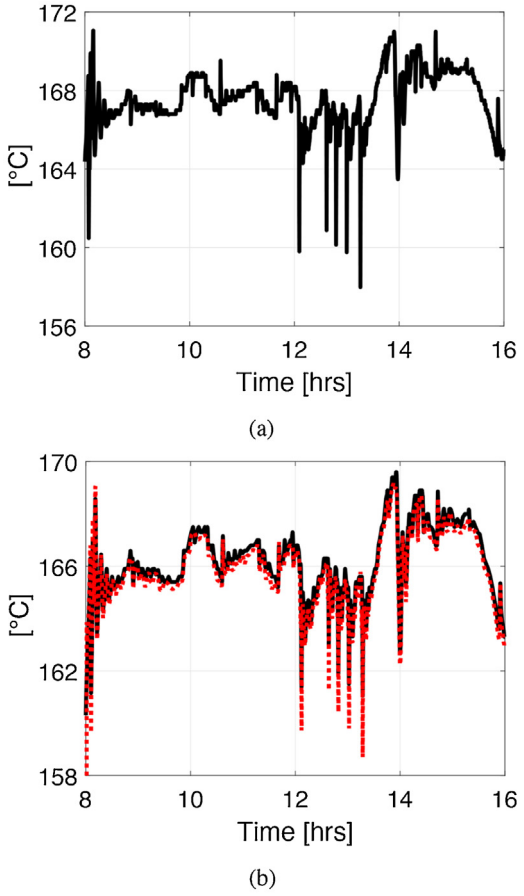

Fig. 6. Validation of the hot water pipe model: (a) input temperature, (b) measured output temperature (solid line), output temperature of the model (dotted line).

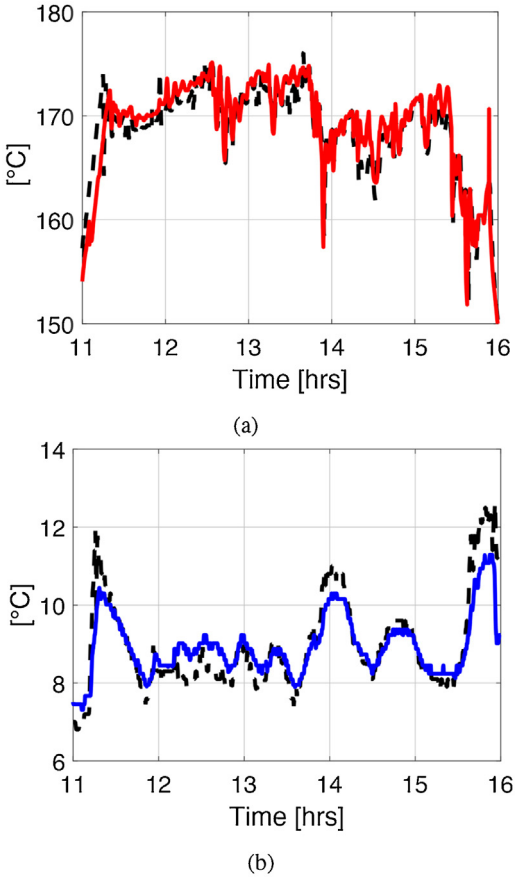

Fig. 7. Validation of the chiller identified models: (a) hot water output temperature, (b) cold water output temperature: measured (dotted line) and model responses (solid line).

as the one of the transport delay, compared to the main dynamics of the system.Also in this case, finite spatial differencing has been used, by considering pipes as formed by the series of elementary volumes of length $0.1m$. The validation transients concerning part of the hot water pipes are depicted in Fig. 6, together with the input temperature used for the experiment. It can be noticed that also in this case the model guarantees a very good fit of the real output (NMSE = 1.64%).

3.4. Chiller

The double effect chiller has two stages of generation to separate the refrigerant from the absorbent for increased overall efficiency. Physical models of this system are available in the literature, see e.g. [24], [25]. However, they are quite complex, difficult to tune, and too detailed for the purpose of this work; for these reasons a black-box identification approach has been adopted. To this end, the following assumptions have been introduced: (i) the hot and cold water cycles are thermally decoupled, (ii) the contribution of the ambient temperature to the thermal exchanges inside the chiller is negligible, (iii) the gas flow, when the chiller is in gas mode, can be considered constant and equal to $q_{gas} = 1.7\text{m}^3\,\text{h}^{-1}$. The operating mode of the chiller has been described by a boolean variable δ_{gas}, with $\delta_{gas} = 1$ if the chiller is in gas mode, while $\delta_{gas} = 0$ otherwise. The gas mode is activated when the component is working ($\delta_{ch} = 1$) and the temperature of the hot water cycle at the input of the chiller is below 165 °C.

Experiments have been performed to estimate the chiller behavior. As a result, it has been possible to conclude that the chiller dynamics is much faster than the one of the temperatures along the pipes and in the storage elements, and it can be assumed to be completely exhausted within the adopted sampling time. Based on these considerations, the chiller has been modeled by two gains, k_{ch}^{hw} for the hot water cycle and k_{ch}^{cw} for the cold water cycle, that take fixed values at any operating condition specified by its status (variables $\delta_{ch}, \delta_{gas}$) and by the water flow rates, which can take only a finite number of values, as described in the following Section 4.1. In conclusion, denoting by $T_{ch}^{hw,in}, T_{ch}^{hw,out}$ the input and output temperatures of the hot water cycle, and by $T_{ch}^{cw,in}, T_{ch}^{cw,out}$ the input and output temperatures of the cold water cycle, the chiller model is

$$T_{ch}^{hw,out}(t) = k_{ch}^{hw}(q_{hw}, \delta_{ch}, \delta_{gas})\, T_{ch}^{hw,in}(t) \tag{5}$$

$$T_{ch}^{cw,out}(t) = k_{ch}^{cw}(q_{cw}, \delta_{ch})\, T_{ch}^{cw,in}(t) \tag{6}$$

where the gains k_{ch}^{hw}, k_{ch}^{cw} have been estimated starting from experimental data. Results of some validation tests, reported in Fig. 7, witness the satisfactory performances of the identified model (NMSE = 14.8%).

The minimization of the electric power consumption is one of the main goals of the control system to be designed, therefore its model must be derived. The main source of electrical consumption is due to the absorption chiller and to its evaporating tower; however, a detailed model goes beyond the purposes of this work. Therefore, a simplified model of the consumed electrical power can be expressed as a linear function of the sum of the refrigeration power ($\dot{Q}_{cw}$), of the consumed gas power ($\dot{Q}_{gas}$), and of the power absorbed by the chiller from the hot water loop ($\dot{Q}_{hw}$), see [21].

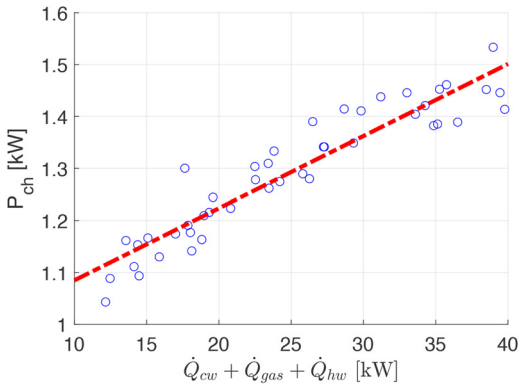

Fig. 8. Chiller power fitting plot.

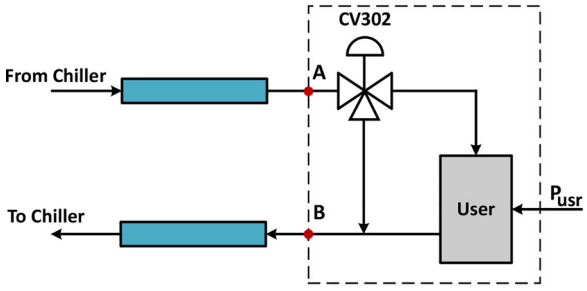

Fig. 9. Structure of the user section of the plant.

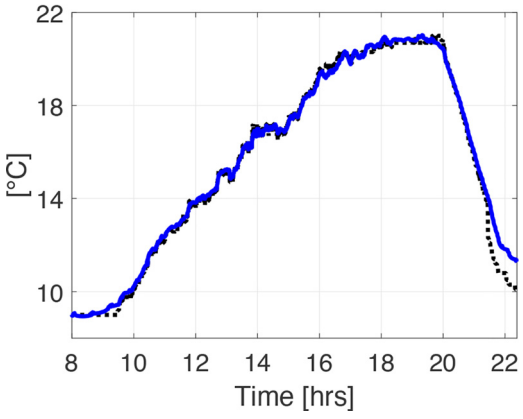

Fig. 10. User model validation. temperature at point B of Fig. 9: measured value (dotted line) and identified model response (solid line).

These powers are expressed as follows

$$\begin{aligned} \dot{Q}_{cw}(t) &= q_{cw} \cdot c_f \cdot (T_{ch}^{cw,in}(t) - T_{ch}^{cw,out}(t)) \\ \dot{Q}_{gas} &= q_{gas} \cdot PCI \\ \dot{Q}_{hw}(t) &= q_{hw}(t) \cdot c_f \cdot (T_{ch}^{hw,in}(t) - T_{ch}^{hw,out}(t)) \end{aligned} \tag{7}$$

where *PCI* is the gross heat of combustion of the natural gas.

The overall power has been modelled as the linear relationship

$$P_{ch}(t) = m(\dot{Q}_{cw}(t) + \dot{Q}_{gas}(t) + \dot{Q}_{hw}(t)) + c \tag{8}$$

where the values of the parameters m and c can be estimated from experimental data, comparing the real electrical consumption with the sum of the powers expressed in (8). Fig. 8 shows several experimental tests that have been carried out on the plant at different operating conditions in order to estimate m and c. For the considered chiller, the estimated values are $m = 0.0139$ and $c = 0.9460$.

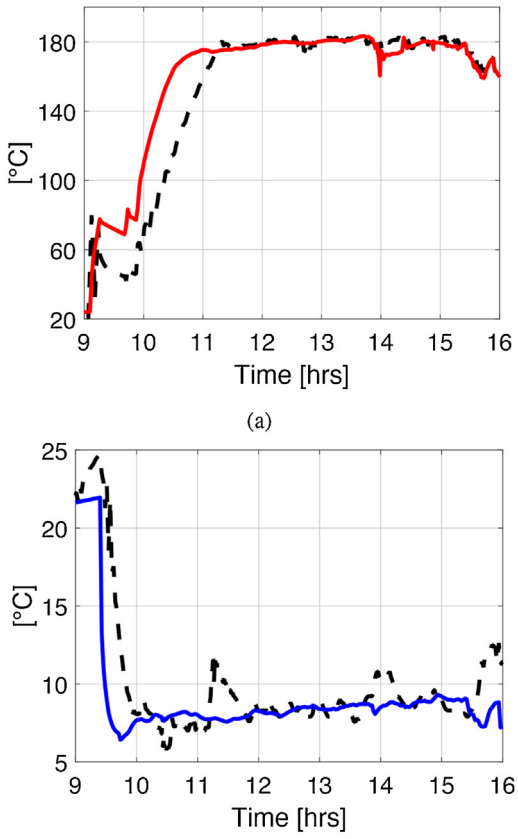

Fig. 11. Validation of the overall model, (a) hot water temperature at the chiller input, (b) cold water temperature at the chiller output. Measured values (dashed lines) and overall model response (solid lines).

3.5. Pump

The variable speed pump can be manipulated in the range $[0–100\%]q^{max}$. However, concerning the hot water loop, it is worth turning the pump off when not necessary, or using it only in the range $[60–100\%]q_{hw}^{\max}$ since the solar collector's efficiency significantly decreases at low flow rates. As already mentioned in Section 2, for the considered solar cooling plant it is not possible to arbitrarily manipulate the cold water flow rate q_{cw}. Being the plant equipped with volumetric pumps, the relationship between their water flow and electric power consumption P_p can be expressed by a simple proportional relationship

$$P_p(t) = k_p \cdot q(t) \tag{9}$$

where k_p is a known parameter and $q(t)$ is the generic water flow.

3.6. User

The model of the user power consumption is required in order to complete the simulator of the system. As mentioned in Section 2 and shown in Fig. 9, the input flow to the user after point A in Fig. 9 is controlled by a PID acting on a valve CV302 depending on the user actual temperature and power requirements. This valve is autonomously manipulated to satisfy the actual user demand and the corresponding controller structure is unknown. Since the objective of our high level controller is to manage the chiller and the storages in order to maintain the cold water temperature at the proper range, it has been reasonable to identify the model of the output temperature T_B at point B of Fig. 9 as function of the input

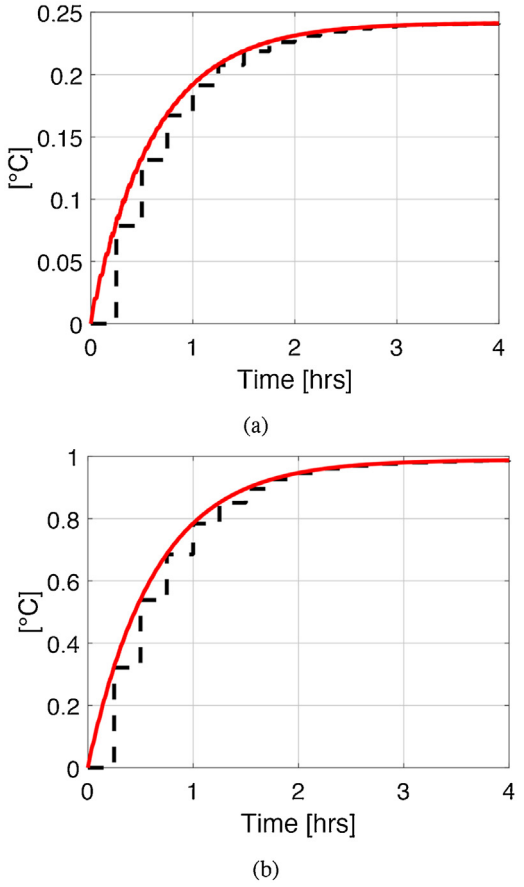

Fig. 12. Responses of the hot water temperature at the chillerinput with the complete and estimated reduced model (11) due to a step variation of: (a) radiation; (b) ambient temperature. Continuous lines: complete model, dashed lines: estimated models.

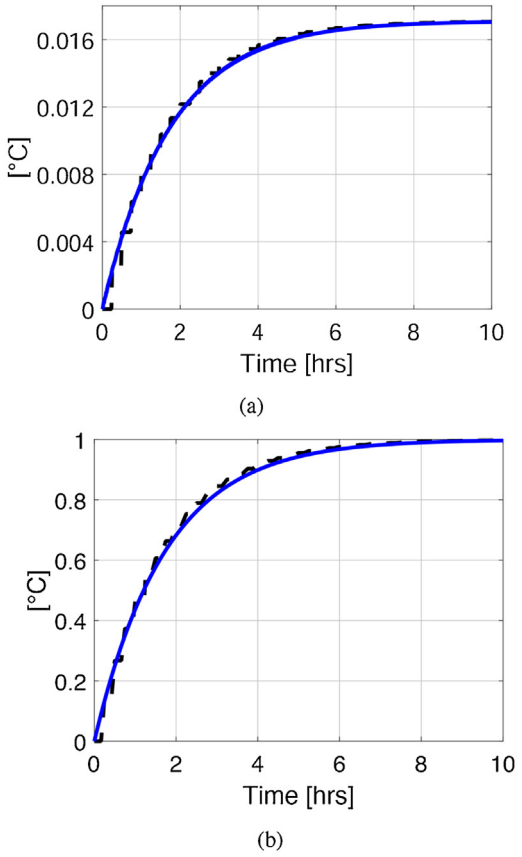

Fig. 13. Responses of the cold water temperature at the chiller output with the complete and estimated discrete model (12) due to a step variation of: (a) user power, (b) ambient temperature. Continuous lines: complete model, dashed lines: estimated model.

temperature T_A at point A and of the power demand by the user P_{usr}. The resulting identified model takes the form

$$T_B(t) = k_B\, T_a(t) + k_P\, P_{usr}(t) \tag{10}$$

where T_e is the temperature of the environment, and the coefficients k_B, k_P have been estimated from data. The validation of the user model is shown in Fig. 10, where a NMSE = 5.9% is achieved.

3.7. Validation of the overall model

The models of the individual components have been implemented in the Matlab/Simulink environment and then assembled to obtain the overall plant model, which has been tested and validated with real data. Note that the resulting model has very high order, due to the spatial discretization adopted to transform the models of the solar collector and pipes into a set of ordinary differential equations. To this regard, consider that the total length of these elements is about 200 m, and that the adopted spatial discretization factor is about 0.1 m. For this reason, the developed simulator is useful for analysis, testing, and validation, but it is not suitable for real-time Model Predictive Control.

Some of the results of this validation phase are shown in Fig. 11. It is apparent that the developed simulator is able to represent with satisfactory accuracy the dynamics of the system. For this reason, it has been used first to obtain the simplified plant model to be used in the control design phase, and then to preliminary test in simulation the control algorithm before implementing it on the real system.

4. Control design

A Hybrid Model Predictive Control (HMPC) algorithm, see [26], has been designed to optimally manage the plant configuration over a future prediction horizon and given the available forecasts of solar radiation and user demand. However, for control design purposes, the model previously described turns out to be too complex, due to its large number of state variables and nonlinearities. For this reason, it has been used to obtain simplified first order linear models by fitting its step responses at different operating conditions and in different configurations.

4.1. Reduced order models

The hot water temperature $T_{ch}^{hw,in}$ at the chiller input and the cold water temperature $T_{ch}^{cw,out}$ at the chiller output are the variables strictly necessary to state the optimization problem described in the following Section 4.2. Therefore, the following first order linear models, expressed in the Laplace transform, have been considered:

$$T_{ch}^{hw,in}(s) = \frac{1}{1+\tau_{hw}(\delta)s}\{\Gamma_I^{hw}(\delta,\delta_{gas},q_{hw})I(s) + + \Gamma_{T_a}^{hw}(\delta,\delta_{gas},q_{hw})T_a(s)\} \tag{11}$$

$$T_{ch}^{cw,out}(s) = \frac{1}{1+\tau_{cw}(\delta)s}\{\Gamma_{T_a}^{cw}(\delta,q_{cw})T_a(s) + \Gamma_{P_{usr}}^{cw}(\delta,q_{cw})P_{usr}(s)\} \tag{12}$$

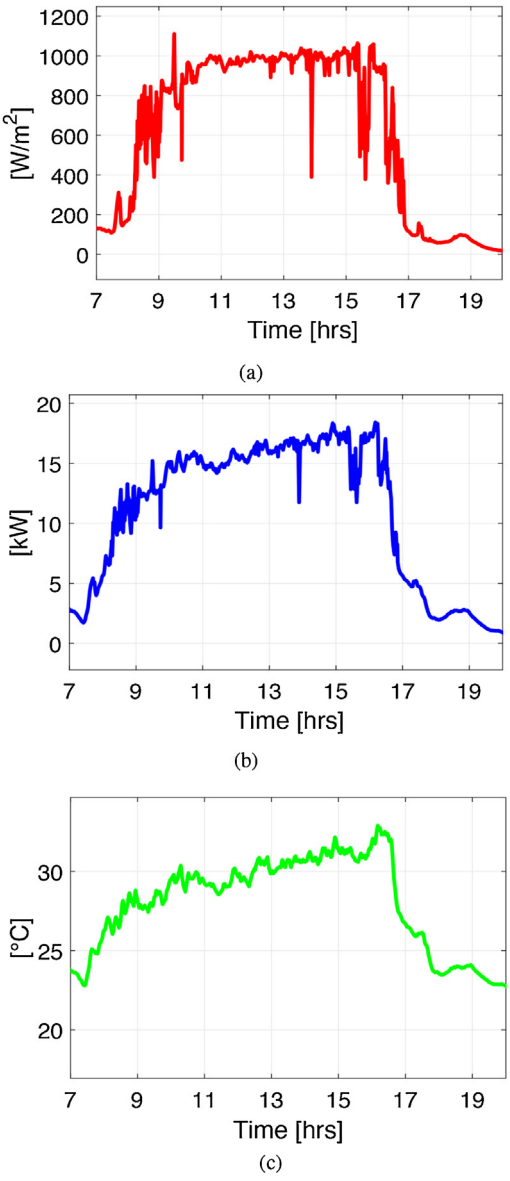

Fig. 14. Transients of (a) the solar radiation, (b) user power demand and (c) ambient temperature for the validation of the estimated reduced model of $T_{ch}^{hw,in}$ and $T_{ch}^{cw,out}$.

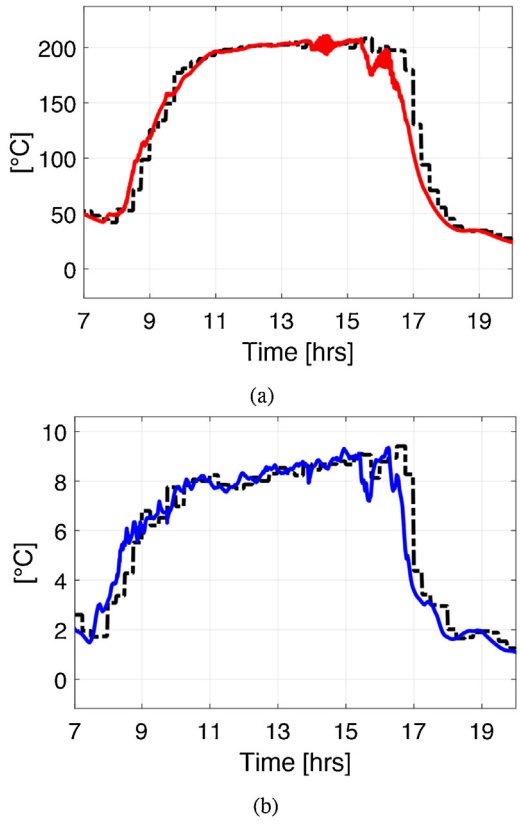

Fig. 15. Reduced model validation: transient of (a) $T_{ch}^{hw,in}$ and (b) $T_{ch}^{cw,out}$ computed with the original model (continuous line) and with the estimated one (stair-wise line).

where the time constants τ_{hw}, τ_{cw} and the gains Γ_I^{hw}, $\Gamma_{T_a}^{hw}$, $\Gamma_{T_a}^{cw}$, $\Gamma_{P_{usr}}^{cw}$ depend on the specific configuration, defined by δ and δ_{gas}, and on the hot water flow rate q_{hw}. Their values have been obtained as follows: for any fixed configuration and for fixed values of the flow rates, starting from steady-state conditions, the inputs I, T_a, P_{usr} have been given a step variation, one at a time. Then, the values of the time constants and of the gains of models (11), (12), have been computed according to a least squares approach minimizing the mean square error between the simulator and the models outputs.

Note that, when the storage elements are included into the hot and/or cold water loops, i.e. when $\delta_{ht} = 1$ and/or $\delta_{ct} = 1$, the tanks dynamics are implicitly included into the models (11), (12). In the other cases, i.e. when $\delta_{ht} = 0$ and/or $\delta_{ct} = 0$, the temperatures inside the tanks evolve according to the first order models (3), (4).

The estimated models have been discretized with the ZOH transformation, see [20], sampling time $\tau = 15$ min, and have been used in the design and implementation of the hybrid predictive controller. Figs. 12 and 13 show some comparisons between the variations of the variables $T_{ch}^{hw,in}$ and $T_{ch}^{cw,out}$ provided by the simulator and the outputs of the identified and discretized systems. These results witness the good prediction properties of the computed reduced order models. As an additional validation result, the responses of the simplified and discretized model and of the overall nonlinear simulator have been compared in front of contemporary variations of I, T_a and P_{usr}. The transients of $T_{ch}^{hw,in}$ and $T_{ch}^{cw,out}$ are shown in Fig. 15, considering the external disturbances reported in Fig. 14 and the fixed plant configuration where the chiller is kept on and the storages are disconnected. It is evident that the computed simplified reduced model satisfactorily resembles the original system dynamics.

The discretized version of equations (3), (4), (11), (12) describes a Mixed-Logical Dynamical (MLD) model, given the presence of both continuous and boolean variables. Although this system is much simpler than the accurate plant model derived in Section 3, in the implementation of the HMPC algorithm there is still a computational issue given by the nonlinear dependency between its gains and the hot water flow q_{hw}. To solve this problem, an additional simplification has been introduced assuming that the flow q_{hw} can only take one of m predefined values $q_{hw,i}$ in a finite set

$$q_{hw,i} \in \{q_{hw,1} = q_{hw}^{\min}, \ldots, q_{hw,m} = q_{hw}^{\max}\}$$

Each flow level $q_{hw,i}$ is then associated to a boolean variable δ_i^q such that

$$\begin{cases} \delta_i^q = 1 & \text{if} \quad q_{hw} = q_{hw,i} \\ \delta_i^q = 0 & \text{otherwise} \end{cases}, \quad \sum_{i=1}^{m} \delta_i^q = 1 \tag{13}$$

At this stage, each gain $\Gamma \in \{\Gamma_I^{hw}, \Gamma_{T_a}^{hw}, \Gamma_{T_a}^{cw}, \Gamma_{P_{usr}}^{cw}\}$ can be defined as:

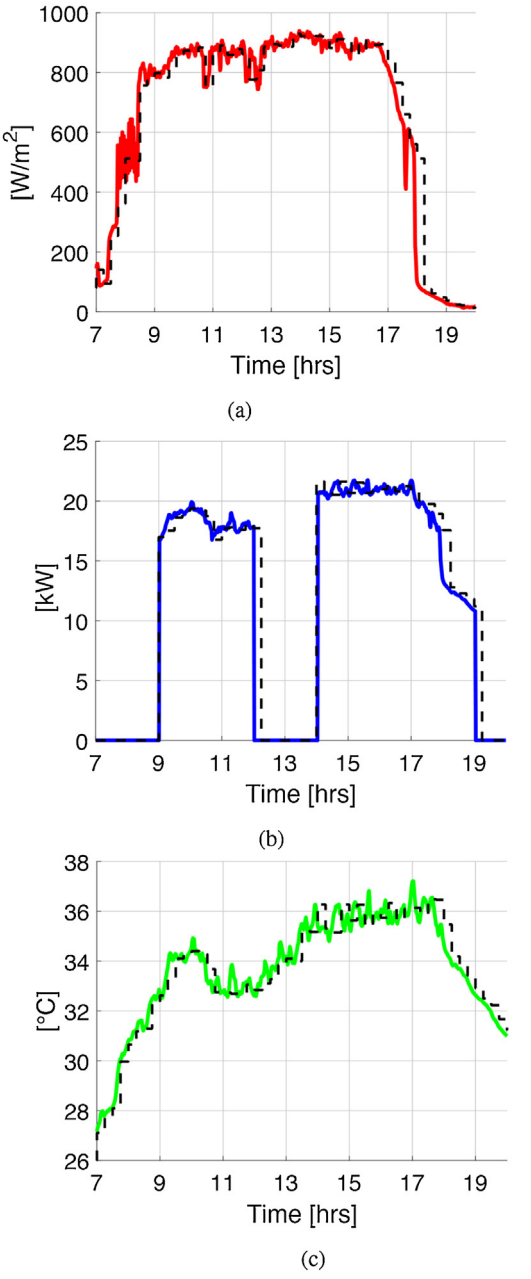

Fig. 16. Simulation test – (a) Solar radiation, (b) user power demand, (c) ambient temperature: real (solid line) and forecast (dashed line).

$$\Gamma(\delta, q_{hw}) = \sum_{i=1}^{m} \Gamma(\delta, q_{hw,i}) \cdot \delta_i^q \tag{14}$$

where now $\Gamma(\delta, q_{hw,i})$ are constants depending on the specific values $q_{hw,i}$ and on the system parameters. Substituting (14) into the reduced model equations (11), (12), the overall model is still nonlinear given the products between continuous and boolean variables. Nevertheless, this type of nonlinearity can be described by a MLD model as explained in [26]. Notably, this task can be well performed by means of the software environment Hysdel, see [27].

4.2. The optimization problem

The HMPC algorithm, running with sampling period $\tau = 15$ min, is designed to minimize at any (discrete-time) instant k and over a prediction horizon of N steps, the electrical and gas consumption, keeping the temperatures of both loops in the required working

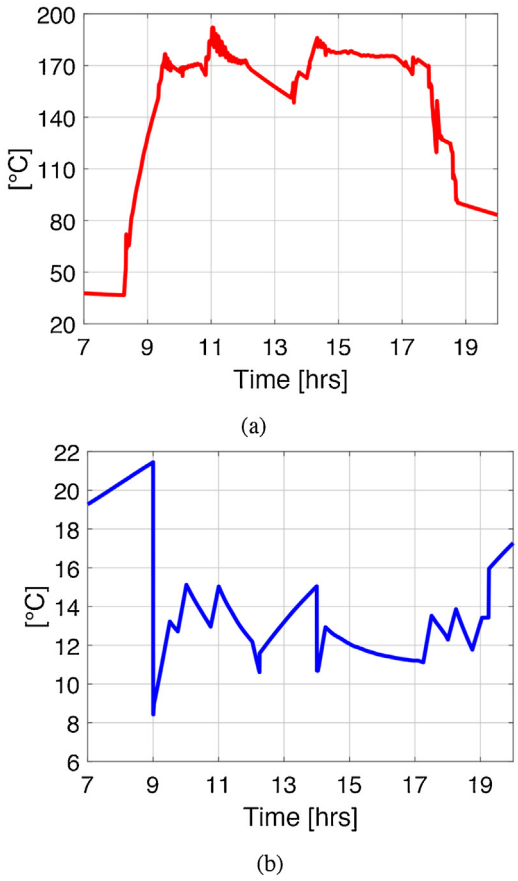

Fig. 17. Simulation test – (a) Hot water temperature at the chiller input, (b) Cold water temperature at the chiller output.

range despite the time-varying user absorption and solar radiation. To this end, let

$$u(k+l) = [\delta(k+l),\ \delta^q_{1,\dots,m}(k+l)], \quad l = 0, \dots, N-1 \tag{15}$$

be the vector of control variables along the prediction horizon and define

$$U(k) = \begin{bmatrix} u(k) & \cdots & u(k+N-1) \end{bmatrix}$$

Then, recalling the expressions of the electrical consumptions of the chiller and of the pump given by (8) and (9), respectively, at any time $\bar{k}$ the following optimization problem is solved:

$$\min_{\epsilon, U(k)} \sum_{k=\bar{k}}^{\bar{k}+N} [w_{ch} \cdot P_{ch}(k) + w_p \cdot P_p(k) + w_g \cdot q_g \cdot \delta_{gas}(k) + w_\epsilon \cdot \epsilon]$$

subject to

$$\begin{cases} Discretized reduced order model equations(11) - -(14) \\ T_{ch}^{hw,in}(k) \le T_{hw}^{\max} + \epsilon \\ T_{ch}^{cw,out}(k) \le T_{cw}^{\max} + \epsilon \\ T_{ch}^{cw,out}(k) \ge T_{cw}^{\min} - \epsilon \\ \epsilon \ge 0 \end{cases}$$

In the cost function, the weights w_{ch}, w_p, w_g are set such that each variable is expressed in equivalent consumed primary energy (kWh), while the slack variable ϵ, with suitably weight w_ϵ, is introduced to guarantee feasibility at any time step, see [28].

The constraints concern the system equations and the requirement of keeping the water loop temperatures in specified ranges.

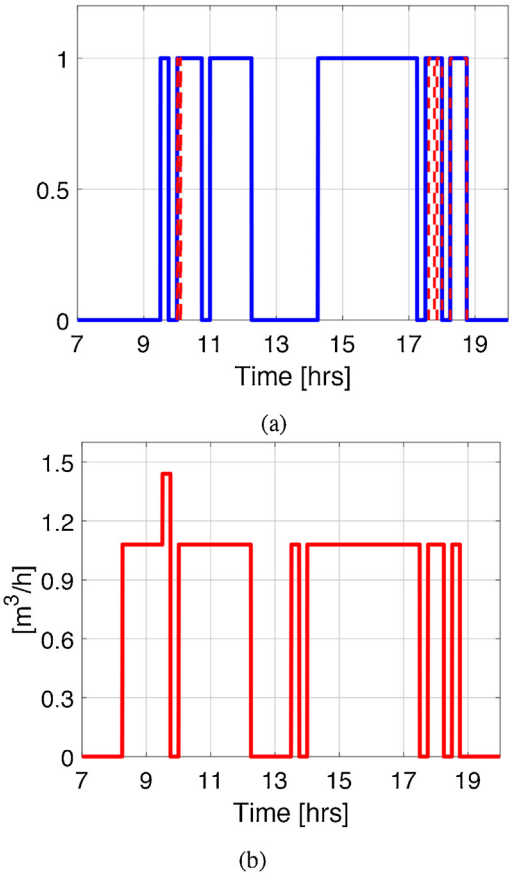

Fig. 18. Simulation test – (a) Chiller: δ_{ch} status (solid line) and δ_{gas} status (dashed line), (b) Hot water flow.

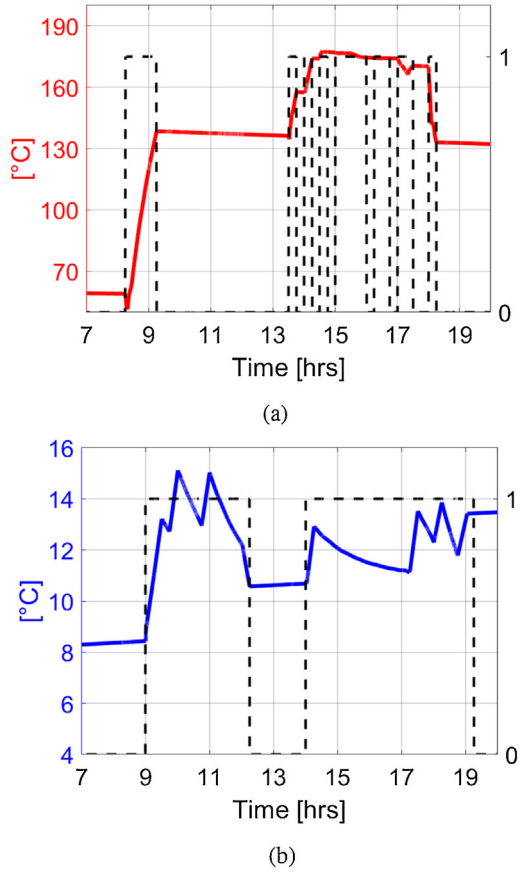

Fig. 19. Simulation test – (a) Hot tank: δ_{ht} status (dashed line, scaled) and internal temperature (solid line), (b) Cold tank: δ_{ct} status (dashed line, scaled) and internal temperature (solid line).

Actually, for the considered plant, the hot water temperature should be below 200 °C, while the cold water temperature should be kept between 4 °C and 20 °C in order to properly satisfy the user demand. However, since the HMPC problem is based on an approximate and simplified model, it has been chosen to put more stringent bounds and to express these requirements as soft constraints through the use of the slack variable ϵ. Therefore, for the HMPC optimization problem implementation, the following bounds have been considered: $T_{hw}^{\max} = 190\,^{\circ}\text{C}$, $T_{cw}^{\max} = 17\,^{\circ}\text{C}$ and $T_{cw}^{\min} = 5\,^{\circ}\text{C}$. In addition, all the constraints on the cold water temperature have been removed when the user demand is null.

Once the optimal solution $U^o(k) = \begin{bmatrix} u^o(k) & \cdots & u^o(k+N-1) \end{bmatrix}$ has been found, only its first element $u^o(k)$ is effectively applied and, according to a receding horizon approach, at time $k+1$ the overall optimization problem is stated and solved again.

5. Simulation and experimental results

The HMPC algorithm has been implemented in a standard Personal Computer (PC) by means of Matlab® equipped with the YALMIP toolbox [29] and with the optimization solver CPLEX®. Its performances have been tested first in simulation with the plant model described in Section 3, also developed in Matlab/Simulink. Then, the algorithm has been used to control the real plant by means of a PLC interfaced with the PC.

5.1. Simulation results

The simulation results concern a summer day with high solar radiation, ambient temperature, and user demand, as shown in Fig. 16. A prediction horizon of 6 hours has been chosen. For the hot water flow, fours levels have been defined, i.e. $q_{hw,1} = 0$, $q_{hw,2} = 0.6\,q_{hw}^{\max}$, $q_{hw,3} = 0.8\,q_{hw}^{\max}$, $q_{hw,4} = q_{hw}^{\max}$ with $q_{hw}^{\max} = 1.8\,\text{m}^3/h$. In the following, all the figures show the plant operations between 7:00 and 20:00, considered the most significant time range both for solar radiation and user demand in tertiary buildings, like the one considered in this work. As it is possible to see from Fig. 17, the HMPC algorithm is able to keep the water temperatures inside their working ranges. Note that the user demand is null in the periods 07:00–09:00, 12:00–14:00, 19:00–20:00, where the constraints on the cold water temperature are automatically deactivated to avoid an unnecessary chiller activity. To maintain the temperatures inside their bounds, the controller properly modifies the plant configuration, i.e. the variables δ_{ch}, δ_{ht}, δ_{ct} and the hot water flow, as shown in Fig. 18, where it is apparent that the chiller tends to use the solar radiation as much as possible, while reducing to the minimum the gas consumption, used mainly when the solar contribution is small, as in the final part of the day (17:00–20:00). The hot and cold water tanks are properly used as effective energy storage elements, as witnessed by the temperatures transients reported in Fig. 19. Note, for example, that the HMPC algorithm tries to store hot water in the tank in the first part of day, so that it can be used in the last part, when the radiation decreases.

5.2. Experimental results

The HMPC algorithm has been tested on the real plant in many days of September 2018; some of the achieved results are presented in the following. Fig. 20 show the prediction and the real solar radiation, user demand, and ambient temperature in one of these

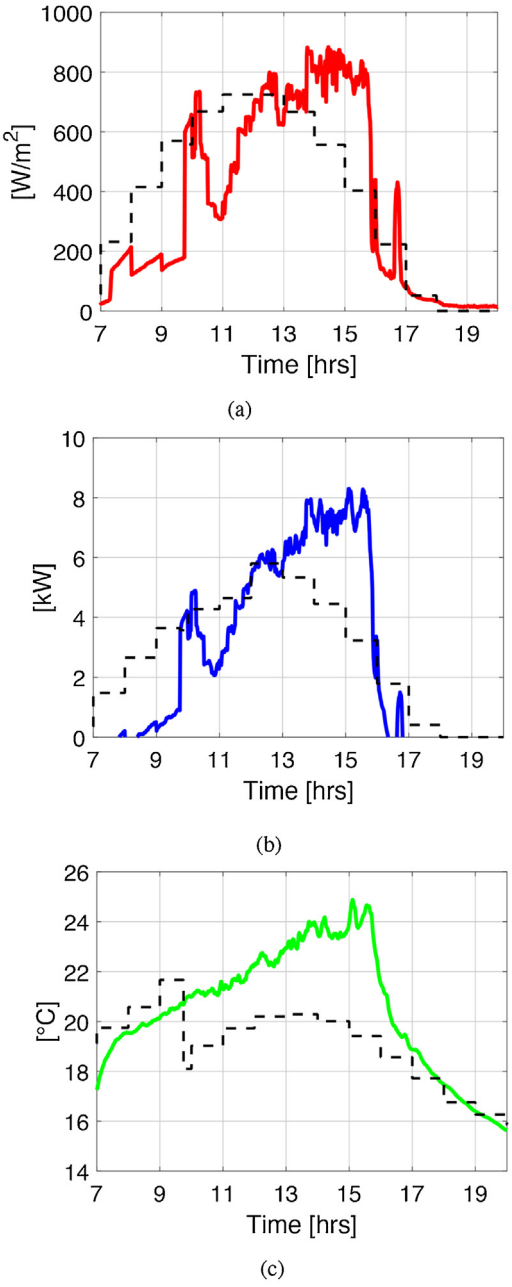

Fig. 20. Real test – (a) Solar radiation, (b) user power demand, (c) ambient temperature: real (solid line) and forecast (dashed line).

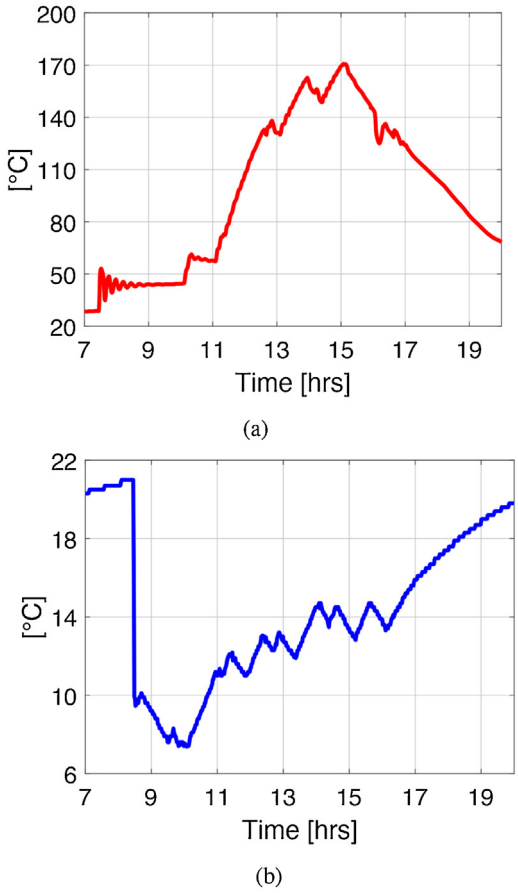

Fig. 21. Real test – (a) Hot water temperature at the chiller input, (b) Cold water temperature at the chiller output.

Table 5
Comparison of gas and electric energy average consumption.

Control strategy	Gas	Electric energy
Relay-based control (simulation)	7.9 m^3	8.25 kWh
HMPC (real tests)	6.2 m^3	6.1 kWh
Saving	22%	26%

days. As it can be noticed, these predictions were not very accurate, so limiting the potential benefits of a predictive approach. The transients of the hot and cold water temperatures are reported in Fig. 21: in order to correctly evaluate these results, it is reminded that that the goal of the control system is not to force the temperatures to track given reference values, but to maintain them in prescribed ranges with limited gas consumption, as indeed it happens when the user demand is not null. In addition, recall that the control system aims to keep the hot water temperature at values greater than 165 °C, so that the chiller can operate in no-gas mode. The oscillatory behaviour of the temperatures, see again Fig. 21, is due to the frequent switch on/off of the chiller aimed at saving energy, as reported in Fig. 22(a), which also shows the chiller's mode of operation (gas/hot water). Since the radiation was not so high during the real tests, as well as the ambient temperature, the chiller was operated for long periods of time in gas mode. The status and temperature of the cold tank are shown in Fig. 23: not surprisingly, the transients of the temperature of the cold water at the chiller output and of the one inside the cold tank are very similar, since the tank is used in almost all the experiment, see Fig. 21(b) and 23 . Note that the cold tank is mainly used to damp the cold water rises and falls given by the switch on/off of the chiller or by the user demand, which may result in the violation of the temperature constraints. This behavior can be also noticed in the simulation results, as shown in Fig. 19(b). The graph of the hot tank temperature is not reported here, since it was not used by HMPC during the tests. This is due to the fact that in Northern Italy the radiation is not very high in September, so that it was not worth heating such a big tank. The performances of the HMPC algorithm, in terms of energy consumption, have been compared to the ones provided by the previously implemented control strategy, where the chiller is activated/deactivated by a relay controller based on the cold water bounds $T_{cw}^{\min}$ and $T_{cw}^{\max}$, while the plant configuration can be not automatically changed based on the external disturbances. The average gas and electrical consumptions achieved with HMPC over the whole period of tests are shown in Table 5, that also summarizes the performances of the relay-based controller computed through simulations using the same external disturbances and initial tem-

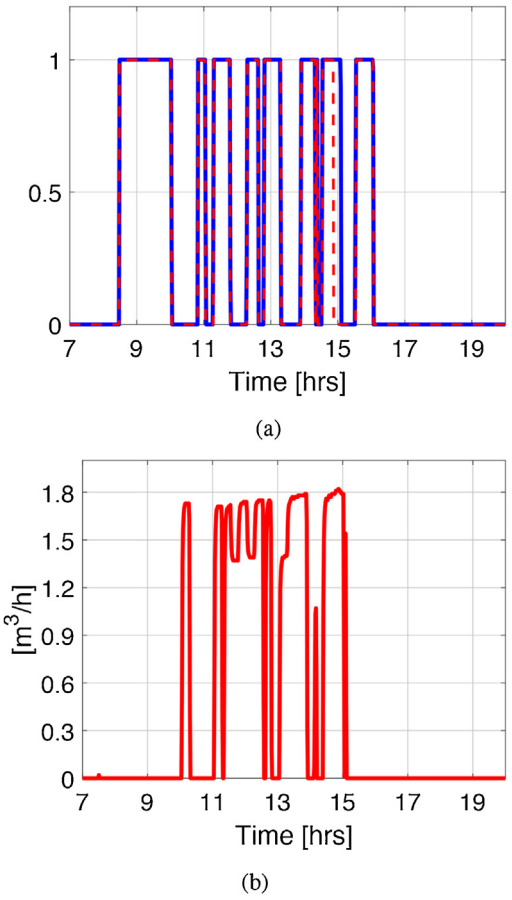

Fig. 22. Real test – (a) Chiller: δ_{ch} status (solid line) and δ_{gas} status (dashed line), (b) Hot water flow.

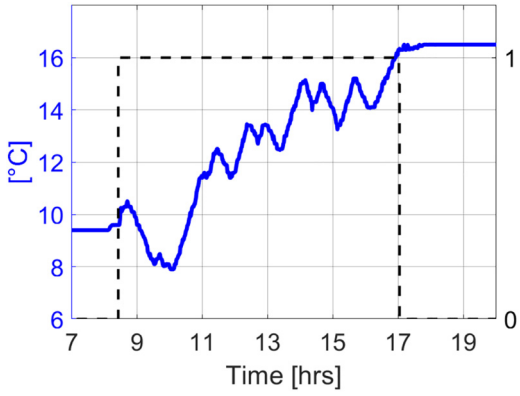

Fig. 23. Reat test – Cold tank: δ_{ct} status (dashed line, scaled) and internal temperature (solid line).

perature conditions. Although during the real tests the weather conditions were not favourable, the HMPC algorithm achieves significant results both in terms of gas consumption reduction and of electric energy saving, mainly due to the efficient management of the chiller activity. Finally, a detailed analysis on the sensitivity of the MPC performance with respect to the quality of the predictions of solar radiation and ambient temperature is reported in [30], which allows to conclude that significant energy savings, with respect to the relay-based control, are achieved with at most 20% prediction errors. Beyond this value, in some cases wrong predictions can lead the MPC controller to select non optimal plant configurations. Notice however that in the reported tests superior performances of HMPC have been obtained, even in presence of larger prediction errors.

6. Conclusions

The complete control design procedure for a solar cooling system has been described in this paper. The modelling and identification phases allowed to obtain a detailed knowledge of the system and to develop an accurate plant simulator. The performances of the designed HMPC controller, evaluated both in simulation and with real tests on the plant, witness the potentialities of the adopted approach. The HMPC controller can easily modulate several control variables, i.e. pumps flow, storage tanks and chiller activity, exploiting the predictions of the solar radiation and user demand, if available. This allows to achieve significant savings in terms of electrical energy and gas consumption. Future developments may regard the redefinition of the mixed-integer optimization problem and of the MLD high-level model used in the MPC design such that it is possible to extend the prediction horizon to the whole day in order to achieve a more efficient overall system management.

References

[1] L. Pérez-Lombard, J. Ortiz, C. Pout, A review on buildings energy consumption information, Energy Build. 40 (3) (2008) 394–398.
[2] G. Grossman, Solar-powered systems for cooling, dehumidification and air-conditioning, Solar Energy 72 (1) (2002) 53–62.
[3] I. Sarbu, C. Sebarchievici, Review of solar refrigeration and cooling systems, Energy Build. 67 (2013) 286–297.
[4] A. Allouhi, T. Kousksou, A. Jamil, P. Bruel, Y. Mourad, Y. Zeraouli, Solar driven cooling systems: an updated review, Renew. Sustain. Energy Rev. 44 (2015) 159–181.
[5] E.F. Camacho, M. Berenguel, F. Rubio, D. Martinez, Control of Solar Energy Systems, Springer London Limited, 2014.
[6] S. Pintaldi, C. Perfumo, S. Sethuvenkatraman, S. White, G. Rosengarten, A review of thermal energy storage technologies and control approaches for solar cooling, Renew. Sustain. Energy Rev. 41 (2015) 975–995.
[7] A. Rossetti, Performance analysis of an advanced variable configuration solar cooling plant with an mpc controller, part a: model and validation, Int. J. Refrig. 93 (2018) 212–223.
[8] M. Rodríguez, C. De Prada, F. Capraro, S. Cristea, Logic embedded nmpc of a solar air conditioning plant, Eur. J. Control 14 (6) (2008) 484–500.
[9] P. Menchinelli, A. Bemporad, Hybrid model predictive control of a solar air conditioning plant, Eur. J. Control 14 (6) (2008) 501–515.
[10] D. Zambrano, W. Garcia-Gabin, Hierarchical control of a hybrid solar air conditioning plant, Eur. J. Control 14 (6) (2008) 464–483.
[11] P. Bermejo, F.J. Pino, F. Rosa, Solar absorption cooling plant in Seville, Solar Energy 84 (8) (2010) 1503–1512.
[12] C. Sonntag, H. Ding, S. Engell, Supervisory control of a solar air conditioning plant with hybrid dynamics, Eur. J. Control 14 (6) (2008) 451–463.
[13] M. Pasamontes, J. Álvarez, J. Guzman, M. Berenguel, E. Camacho, Hybrid modeling of a solar-thermal heating facility, Solar Energy 97 (2013) 577–590.
[14] J. Álvarez, M. Pasamontes, J. Guzmán, E. Camacho, A practical hybrid predictive control algorithm for a low-temperature thermosolar plant, Optim. Control Appl. Methods 37 (3) (2016) 508–520.
[15] H. Scherer, M. Pasamontes, J. Guzmán, J. Álvarez, E. Camponogara, J. Normey-Rico, Efficient building energy management using distributed model predictive control, J. Process Control 24 (6) (2014) 740–749.
[16] H. Scherer, E. Camponogara, J. Normey-Rico, J.D. Álvarez, J.L. Guzmán, Distributed mpc for resource-constrained control systems, Optim. Control Appl. Methods 36 (3) (2015) 272–291.
[17] E. Herrera, R. Bourdais, H. Guéguen, Predictive and interactive controllers for solar absorption cooling systems in buildings, J. Process Control 24 (6) (2014) 836–845.
[18] E. Herrera, R. Bourdais, H. Guéguen, A hybrid predictive control approach for the management of an energy production-consumption system applied to a trnsys solar absorption cooling system for thermal comfort in buildings, Energy Build. 104 (2015) 47–56.
[19] R.W. Saaty, The analytic hierarchy process-what it is and how it is used, Math. Model. 9 (3–5) (1987) 161–176.
[20] K.J. Åström, B. Wittenmark, Computer-Controlled Systems: Theory and Design, Courier Corporation, 2013.
[21] A. Rossetti, E. Paci, G. Alimonti, Experimental analysis of the performance of a medium temperature solar cooling plant, Int. J. Refrig. 80 (2017) 264–273.
[22] E. Camacho, F. Rubio, M. Berenguel, L. Valenzuela, A survey on control schemes for distributed solar collector fields. part i: Modeling and basic control approaches, Solar Energy 81 (10) (2007) 1240–1251.
[23] P.J. Thomas, Simulation of Industrial Processes for Control Engineers, Elsevier, 1999.

[24] S. Bittanti, A. De Marco, M. Giannatempo, V. Prandoni, A dynamic model of an absorption chiller for air conditioning, in: International Conference on Renewable Energies and Power Quality, (ECREPQ'10), Granada, Spain. European Association for the Development of Renewable Energies, 2010.
[25] C. Vasilescu, D. Hera, C.I. Ferreira, Model for double-effect absorption refrigeration cycle, Termotehnica 2 (2011) 43–48.
[26] A. Bemporad, M. Morari, Control of systems integrating logic, dynamics, and constraints, Automatica 35 (3) (1999) 407–427.
[27] F.D. Torrisi, A. Bemporad, Hysdel-a tool for generating computational hybrid models for analysis and synthesis problems, IEEE Trans. Control Syst. Technol. 12 (2) (2004) 235–249.
[28] J. Maciejowski, Predictive Control With Constraints, Pearson education, 2002.
[29] J. Lofberg, Yalmip: A toolbox for modeling and optimization in matlab, in: 2004 IEEE International Symposium on Computer Aided Control Systems Design, IEEE, 2004, pp. 284–289.
[30] C. Sandroni, A. Rossetti, Medium temperature solar cooling plants: experimental investigation of a variable configuration plant and study of innovative solutions, Report Power System Research 17001375, http://www.rse-web.it/documenti/documento/317719.